Chemical Physics 357 (2009) 188–197

Contents lists available at ScienceDirect

Chemical Physics

journal homepage: www.elsevier.com/locate/chemphys

Structural model and excitonic properties of the dimeric RC–LH1–PufX complex from *Rhodobacter sphaeroides*

Melih Şener [a,b,1], Jen Hsin [a,b,1], Leonardo G. Trabuco [a,c], Elizabeth Villa [a,c], Pu Qian [d], C. Neil Hunter [d], Klaus Schulten [a,b,*]

[a] Beckman Institute, University of Illinois at Urbana-Champaign, 405 N. Mathews Ave, Urbana, IL 61801, United States
[b] Department of Physics, University of Illinois at Urbana-Champaign, Urbana, IL 61801, United States
[c] Center for Biophysics and Computational Biology, University of Illinois at Urbana-Champaign, Urbana, IL 61801, United States
[d] Department of Molecular Biology and Biotechnology, University of Sheffield, Sheffield S10 2TN, UK

ARTICLE INFO

Article history:
Received 4 September 2008
Accepted 9 January 2009
Available online 14 January 2009

Keywords:
Photosynthesis
Membrane curvature
Molecular dynamics/flexible fitting
Excitons
Purple bacteria
Reaction center

ABSTRACT

The light-harvesting apparatus of the purple bacterial photosynthetic unit consists of a pool of peripheral light-harvesting complexes that transfer excitation energy to a reaction center (RC) via the surrounding pigment–protein complex LH1. Recent electron microscopy and atomic force microscopy studies have revealed that RC–LH1 units of *Rhodobacter (Rba.) sphaeroides* form membrane-bending dimeric complexes together with the polypeptide PufX. We present a structural model for these RC–LH1–PufX dimeric complexes constructed using the molecular dynamics flexible fitting method based on an EM density map. The arrangement of the LH1 BChls displays a distortion near the proposed location of the PufX polypeptide. The resulting atomic model for BChl arrays is used to compute the excitonic properties of the dimeric RC–LH1 complex. A comparison is presented between the structural and excitonic features of the S-shaped dimeric BChl array of *Rba. sphaeroides* and the circular BChl arrangement found in other purple bacteria.

1. Introduction

Photosynthetic light harvesting is achieved by the cooperation of up to hundreds of proteins containing thousands of pigments capturing and transferring light energy for subsequent conversion to stable chemical energy [1–6]. This conversion is initiated at a reaction center (RC) that utilizes the electronic excitations received from the surrounding pigment pool for transmembrane electron transfer (for reviews see Refs. [7–14]). The charge gradient thus created is converted to chemical energy in either oxygenic or anoxygenic photosynthetic processes, the latter being governed by evolutionarily more primitive systems [15]. The anoxygenic purple bacterial photosynthetic unit (PSU) constitutes a remarkably simpler light-harvesting system than those found in cyanobacteria and plants. The atomic structure of purple bacterial RCs [16–20] and their surrounding light-harvesting antennae [21–27] permitted the elucidation of the light-harvesting process down to a quantum mechanical level [28–49,9,50]. Furthermore, the supramolecular organization of the participating photosynthetic proteins has been investigated in experimental [51–56,20,57–59] and theoretical [60–63,50] studies.

The purple bacterial PSU from *Rhodobacter (Rba.) sphaeroides* consists mainly of a peripheral pool of light-harvesting complex II (LH2) units that surrounds arrays of reaction center–light-harvesting complex I–PufX (RC–LH1–PufX) dimers which induce membrane curvature [64]. The dimeric architecture of RC–LH1–PufX units of *Rba. sphaeroides* [59] is not realized in other purple bacteria, such as *Rhodospirillum rubrum* [52], that involve only monomeric RC–LH1 complexes. Further constituents of the PSU are the bc_1 complex [65–68], cytochrome c_2, and ATP synthase [69–71], which jointly convert the charge gradient, created after light harvesting by the LH2 and RC–LH1–PufX units, into stable chemical energy in the form of ATP.

The PSU is spatially organized into lamellar or spherical pseudo-organelles. The respective membrane curvature induced by the constituent pigment–protein complexes of the PSU is essential for photosynthetic function. A recent molecular dynamics (MD) study of the photosynthetic membranes in *Rba. sphaeroides* revealed that intrinsic curvature is spontaneously induced by an array of membrane-embedded LH2 units, whereas an initially flat RC–LH1–PufX dimer spontaneously bends at the dimerization junction [64]. Single-particle electron microscopy (EM) analysis of negatively stained RC–LH1–PufX dimeric complexes in *Rba. sphaeroides* displayed bending between RC–LH1 monomers [59]. The curvature

* Corresponding author. Address: Beckman Institute, University of Illinois at Urbana-Champaign, 405 N. Mathews Ave, Urbana, IL 61801, United States. Tel.: +1 217 244 1604; fax: +1 217 244 6078.
E-mail address: kschulte@ks.uiuc.edu (K. Schulten).
[1] These authors have contributed equally to this manuscript.

0301-0104/$ - see front matter © 2009 Elsevier B.V. All rights reserved.
doi:10.1016/j.chemphys.2009.01.003

of the photosynthetic membrane induced by these pigment–protein complexes increases the effective surface area per unit volume available for light harvesting and likely optimizes the electrostatic and chemiosmotic potentials governing energy conversion as suggested recently in view of the observed curvature around ATP synthase dimers [72]. As a result of the induced curvature, the PSU of *Rba. sphaeroides* forms pseudo-spherical invaginations of the inner membrane with a diameter of approximately 70 nm [50]. The resulting volume of the vesicle ensures the necessary cytochrome c_2 concentration to reduce the RCs and the proton concentration to drive the ATP synthase.

Recent coarse-grained Monte Carlo studies modeled the spontaneous generation of photosynthetic vesicles due to the accumulation of curvature by its constituents [73]. An atomic level description of such a photosynthetic vesicle for *Rba. sphaeroides* was presented in [50], based on atomic force microscopy (AFM) [53,54,56,20,58], cryo-EM [51,52,55,57], and linear dichroism [56] data as well as on available atomic structures of the constituent proteins. This description elucidated the quantum mechanical basis of efficient light harvesting across an entire photosynthetic membrane entailing about 200 proteins and 4000 bacteriochlorophylls (BChls) [50].

The aforementioned theoretical studies [60–63,50,73,64] constitute the first steps toward a comprehensive biology of the PSU by combining spectroscopy, structure, and energy transfer dynamics data with a multitude of simulation techniques, bridging length scales of 10^0–10^4 Å (atomic to vesicular sizes) and time scales of 10^{-15}–10^{-3} s (inter-pigment excitation hopping to vesicle curvature formation times).

Accurate vesicle-scale structural models of the PSU require the availability of the atomic structures of the constituent molecules. Unfortunately, no atomic structure is currently available for the membrane-bending dimeric S-shaped RC–LH1–PufX complex of *Rba. sphaeroides*. In an earlier study of *Rba. sphaeroides* vesicles [50] a planar model of the dimeric RC–LH1–PufX BChl array was constructed based on single-particle EM analysis [57] available at the time. However, recent data collected from electron micrographs of over 4000 negatively stained dimer particles enabled the reconstruction of a 3D map of the dimer complex at 25 Å resolution. This map [59] indicates that the RC–LH1–PufX dimer exhibits a bending angle of 146° at the dimerization junction.

In the current study as well as in a complimentary study [74], we present an atomic structural model for the *Rba. sphaeroides* RC–LH1–PufX complex based on single-particle EM analysis [59]. The structural model is obtained using the molecular dynamics flexible fitting (MDFF) method [75] already successfully applied to the ribosome, but under vacuum conditions [76]. The MDFF methodology combines in the present case the MD simulation of an earlier planar model of the RC–LH1–PufX complex [50,64] in a membrane-water environment with the observed 3D cryo-EM map [59], introducing the latter into the MD force field [75]. The resulting all-atom model not only elucidates the structural basis of the membrane-bending curvature of the complex, but also provides information on the spatial arrangement of the BChl array of RC–LH1–PufX dimers. The geometry of the BChl array thus established permits on the one hand the calculation of the excitonic properties of the complex following the effective Hamiltonian approach [37–40,77,45,42–44,78,79,48,49,9,80,81,50] and on the other hand description of RC–LH1–PufX dimers forming vesicles and tubes [74]. Altogether the broad purpose of the current study is then twofold: first, to explore the geometry of the BChl array in the dimeric RC–LH1–PufX complex; second, to determine computationally the ramifications of this geometry for the quantum biological characteristics of the system.

The organization of this paper is as follows. First, the MDFF protocol employed for the generation of the atomic structural model for the RC–LH1–PufX dimer is described in detail. Then the effective Hamiltonian formulation for the BChls of the RC–LH1–PufX dimer is introduced as the basis of the excitonic structure computations for the BChl array obtained by the MDFF study and applied to determine the spectral properties and excitation transfer dynamics of the complex.

2. Methods

2.1. Molecular dynamics flexible fitting of the RC–LH1–PufX dimer

MDFF is a modeling technique which uses a MD simulation to flexibly fit atomic structures into electron microscopy maps [75]. In an MDFF simulation, two external potentials (U_{EM}, U_{SS}) are applied to the system in addition to the usual MD potential (U_{MD}). Thus, the total energy of the simulated system is

$$U_{total} = U_{MD} + U_{EM} + U_{SS}, \quad (1)$$

where U_{MD} refers to the molecular dynamics force field, U_{EM} is derived from the EM density map to steer the atoms toward filling the regions with high observed density, and U_{SS} is a harmonic potential that preserves the secondary structure to prevent overfitting.

The MDFF method requires a starting atomic model for the constituents that are being fitted to the target EM density map. A planar atomic model for the RC–LH1–PufX dimer of *Rba. sphaeroides* was provided in [64] based on available solution structures and 2D EM projection data [57]. As described in [64], an NMR solution structure (PDB id: 1DX7) [25] was used for the LH1 β-apoprotein. For the LH1 α-apoprotein a homology model was built in the absence of an available structure based on the *Rhodospirillum rubrum* LH1 α-apoprotein reported in [82]. The bacteriochlorophyll and carotenoid molecules were then placed in between the α/β-apoprotein pair to form an LH1 subunit, their positions chosen to be similar to those in *Rhodospirillum molischianum* LH2 [24]. This step was followed by energy minimization to ensure proper ligation. The LH1 α/β subunit was then replicated into 28 copies and arranged into an S-shaped dimer based on the cryo-EM data reported in [57]. Two RCs (PDB id: 1PCR [18]) and two PufX proteins [83] were finally placed within the LH1 dimer based on EM data [57] (see [64] for further details of the modeling effort).

The atomic structural model for the RC–LH1–PufX dimer thus constructed in [64] was fitted into the 25 Å resolution 3D EM density map reported in [59] as follows. Rigid-body docking was first performed to place the dimer model inside the EM density using the Situs package [84]. A 320 Å × 170 Å lipid patch composed of 50% POPE and 50% POPG was then positioned around the dimer. The lipid–protein system was solvated in a 350 Å × 200 Å × 140 Å water box. Ions were added at 0.3 M to mimic the physiological environment. The entire solvated and membrane-embedded RC–LH1–PufX dimer system consists of 890,307 atoms. The simulation setup is shown in Fig. 1.

The MDFF simulation was performed using NAMD [85–88]. Parameters for the MD potential (U_{MD}) were taken from the CHARMM27 force field [89] with the CMAP correction [90], water being described by the TIP3P model [91]. Long-range electrostatic forces were evaluated using the particle-mesh Ewald (PME) summation method with a grid size of < 1Å. An integration time step of 1 fs was used with a multiple time-stepping algorithm [92]. Bonded terms were evaluated every time step, with short-range non-bonded terms evaluated every fourth time step. Constant temperature ($T = 300$ K) was maintained using Langevin dynamics, with a damping coefficient of 1 ps^{-1}. A constant pressure of 1 atm was enforced using a Nosé–Hoover Langevin piston with a decay period of 100 fs and time constant of 50 fs.

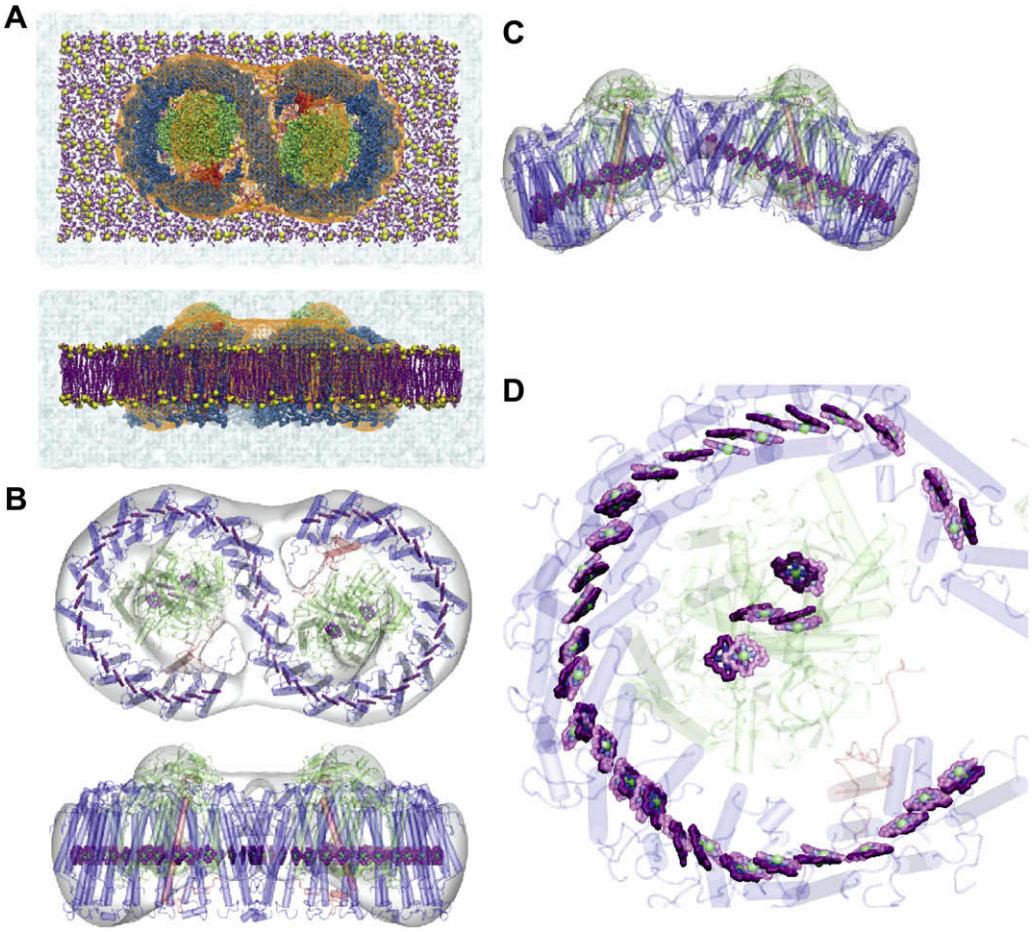

Fig. 1. Structure determination for the dimeric RC–LH1–PufX complex from *Rba. sphaeroides*. The MDFF simulation setup is shown in (A): LH1 in blue, RC in green, PufX in red, dimer density in orange mesh, lipids in purple with the phosphorous atoms shown as yellow spheres, and the water box in transparent blue. (B) Shown is the dimeric complex and its BChls in the initial structure ($t = 0$; for clarity each BChl is represented only by its porphyrin ring). The EM density map is displayed as a transparent surface. (C) Shown is the BChl arrangement after a 17 ns MDFF calculation. The BChl positions, obtained by averaging the last 3 ns of the MDFF trajectory, are shown in (D). The BChl array thus obtained by trajectory averaging was divided into two groups corresponding to each monomer and superimposed over each other (rendered opaque and transparent for the two monomers, respectively). A distortion of the BChl array near the proposed location of PufX can be discerned (cf. Fig. 2E and F). The BChl arrangement used in subsequent calculations was obtained by further averaging the positions and the orientations of BChls from both monomers, resulting in an array with exact C_2-symmetry (cf. Fig. 2).

Only the atoms belonging to the RC–LH1–PufX dimer were coupled to the additional MDFF potentials U_{EM} and U_{SS}. The rest of the system, i.e., lipids, water, and ions, were only subjected to the MD potential U_{MD}. The MDFF potentials U_{EM} and U_{SS} contain adjustable parameters as described in [75]. In the present study, the scaling factor of U_{EM} determining the magnitude of forces applied to the atoms, ξ, was chosen to be 0.3 kcal mol^{-1}, following [75]. The other parameter, k_μ, which is the spring constant of the harmonic restraints applied in U_{SS}, was chosen to be $k_\mu = 200$ kcal mol^{-1} Å^{-2} [75]. The dimer was moved into the EM map [59] within few nanoseconds of the MDFF simulation. The global cross-correlation coefficient improved from 0.75 to 0.80, and the local cross-correlation coefficient, with threshold of 0.1σ above the mean, improved from 0.37 to 0.69.

We note that at a 25 Å resolution of the EM map the accuracy of the final structure is rather limited. For accurate structures an EM map resolution of 7 Å or better is desirable [75]. However, in the present case the main property following from the MDFF analysis of the EM maps is the overall bending of the protein which is a low resolution property that does not require local rearrangement within the protein. Furthermore, the stability of the membrane–protein system obtained by the MDFF method was verified by a subsequent 20 ns equilibrium MD simulation. The resulting membrane curvature observed in the equilibrium MD simulation is consistent with the observed radius of curvature of the chromatophore vesicle in which the dimer complex resides [74]. Given the large scale of the bending effect for the dimer complex, small structural alterations in the initial RC–LH1–PufX model will likely have little effect on the final structure obtained using MDFF.

2.2. Effective Hamiltonian and excitonic properties

Effective Hamiltonian formulations have been successfully employed for a long time to account for the excitonic properties of pigment arrays in purple bacterial as well as other light-harvesting complexes [37–40,77,45,42–44,78,79,48,49,9,80,81,50]. The effective Hamiltonian is typically defined in the basis of the lowest excited state of the BChl molecule, namely the Q_y-excited state [93]. A basis set of local excitations is $|i\rangle = |\phi_1\phi_2\cdots\phi_i^*\cdots\phi_N\rangle$, where only the ith BChl is Q_y-excited and all the other BChls are in their ground states. In this basis the effective Hamiltonian is [37–39,77,44,45,78,48,9]

$$H = \sum_i \epsilon_i |i\rangle\langle i| + \sum_{i\neq j} V_{ij}|i\rangle\langle j|, \tag{2}$$

where ϵ_i is the Q_y-excitation energy of BChl i, the values being assigned so as to reproduce observed exciton spectra [94–96,45,78], and V_{ij} is the electronic coupling between BChls i and j. Over large

(>20 Å) BChl distances, V_{ij} can be evaluated accurately through the induced dipole–induced dipole approximation

$$V_{ij} = (\mathbf{d}_i \cdot \mathbf{d}_j)/r_{ij}^3 - 3(\mathbf{r}_{ij} \cdot \mathbf{d}_i)(\mathbf{r}_{ij} \cdot \mathbf{d}_j)/r_{ij}^5, \quad (3)$$

where $\mathbf{d}_i$ is the transition dipole moment vector for BChl i [97]. For nearest neighbor BChls of LH1, the dipolar approximation (Eq. (3)) yields poor results [12]. Instead, alternating nearest neighbor couplings of 806 cm^{-1} and 377 cm^{-1} are adopted following [45], wherein the couplings were determined based on a fit of the resulting exciton spectrum to quantum chemistry calculations [98]. The coupling between the special pair BChls in the RC is taken to be 500 cm^{-1} [94,45]. All other BChl couplings are computed according to Eq. (3).

The effective Hamiltonian (Eq. (2)) determines both spectral properties and excitation transfer dynamics of the BChl assembly [4,37,42,44,78,79,48,9,80,81,12]. It was demonstrated already over half a century ago by Duysens [6] that an approximate account of excitation transfer dynamics can be achieved in the framework of Förster energy transfer [4] using simply the correct concentration of pigments without specific knowledge of the geometry of the pigment assembly. In fact, already the first treatment of exciton migration among chlorophylls in photosynthesis by Arnold and Oppenheimer was based on chlorophyll concentration as a key parameter (publication [3] stems from a much earlier conference lecture [2]).

The BChls belonging to LH1 and the RC are weakly coupled due to the large distance between them. This spatial separation between the antenna BChl and the BChl of the electron transfer chain is required for 'safe' charge separation at the RC [11,12], i.e., for securing that electrons are transferred towards the quinone binding site, and not towards the light-harvesting chlorophylls. Between two such weakly coupled BChl groups excitation transfer can be described by a generalization of the Förster formula. Accordingly, the total rate of transfer between a donor cluster D of BChls and an acceptor cluster A is [37,99,78,9,100,101,14,13]

$$\mathscr{T}_{DA} = \frac{2\pi}{\hbar} \sum_{m\in D} \sum_{n\in A} \frac{e^{-E_m^D/k_BT}}{\sum_{l\in D} e^{-E_l^D/k_BT}} |V_{mn}^{DA}|^2 \int dE S_m^D(E) S_n^A(E), \quad (4)$$

where E_m^D are the donor energy levels; $S_m^D(E)$ and $S_n^A(E)$ denote the appropriately normalized donor and acceptor spectral lineshapes, respectively; the coupling

$$V_{mn}^{DA} = \sum_{ij} c_{m,i}^D c_{n,j}^A V_{ij} \quad (5)$$

between the donor state m and the acceptor state n depends on the donor eigenvector $c_{m,i}^D$ and the acceptor eigenvector $c_{n,j}^A$ of the respective Hamiltonians; a Boltzmann population of donor states is assumed. The generalized Förster formulation becomes increasingly less accurate in strong coupling regimes ($\sim 10^2$ cm^{-1}) where it should be superseded by the modified Redfield theory [102,79,103,80,81]. The computational complexity of Redfield theory-based approaches limits their usefulness to small pigment arrays (for a survey of these methods see [81]). With the aim of eventually utilizing the current framework for vesicle-scale simulations [50], we adopt in the following the generalized Förster model (Eq. (4)) for excitation transfer computations.

The magnitude of the dipole strengths adopted in Eq. (3) strongly influences excitation transfer rates. In the vesicle-scale PSU study [50] a value of 8.3 Debye was adopted for the effective dipole strengths of BChls uniformly across all LH2, LH1, and RC BChls without differentiating between BChls in different proteins (LH1, RC, LH2). This oversimplification, adopted at the time due to the large system size of nearly 4000 BChls, resulted in an overestimate of both the forward and backward transfer rates between LH1 and RC exciton states [50]. The transfer rates are dependent approximately on the fourth power of individual dipole strengths. In the following, we adopt a value of 5.4 Debye for the effective dipole strength between LH1 and RC BChls. This value reproduces the observed $(8\ ps)^{-1}$ RC → LH1 back transfer rate and is within 15% of the corresponding 6.3 Debye dipole strength reported earlier [32]. The resulting effective Hamiltonian successfully reproduces also the LH1 → RC forward transfer rate and the observed excitonic spectra, as discussed below.

3. Results

In the following, the geometry of the BChl array for the dimeric RC–LH1–PufX complex obtained by the MDFF method and the corresponding excitonic properties of the resulting structure are discussed.

3.1. Geometry of the dimeric RC–LH1–PufX complex

The finite temperature disorder effects, arising naturally in MD simulations, imply that the structural models obtained at the end of an MDFF calculation correspond not to an ordered system such as in crystallography data, but to a particular instance of the protein in its native membrane-water environment subject to thermal disorder. Before a comparison can be made between the MDFF-generated structural model of the RC–LH1–PufX dimer and the atomic structures available for similar pigment–protein complexes, the thermal disorder effects should be minimized.

The geometry of the BChl array can be determined readily since the relevant geometrical quantities are only the center position and the orientation of the BChl porphyrin ring as given by the location of the corresponding central Mg atom and the direction of the N_B–N_D unit vector, respectively. The averages of these quantities, considered to represent the low temperature structure, were taken over the final three nanoseconds of the 17 ns MDFF trajectory that represents an equilibrated structure, as tested through the RMSD of the atomic model (relative to the initial structure) and through cross-correlation to the cryo-EM map (see [75] for a discussion of MDFF convergence). First, the position of the central Mg atom and the orientation vector of the porphyrin ring for each LH1 BChl were averaged. After the averaging of BChl conformations over the trajectory, the two LH1 monomers constituting the S-shaped dimer were superimposed over each other via a least square fit between their BChls as shown in Fig. 1D. The lack of significant deviation of the BChl geometry between the two LH1 monomers is a successful consistency check for the MDFF method as shown in Fig. 1D. The positions and orientations of the BChl arrays from the two monomers were superimposed through the appropriate symmetry operation and averaged. The resulting BChl array was duplicated into two monomers by reflection along the dimer symmetry axis to generate a dimeric LH1 BChl array with an exact C_2-symmetry (cf. Fig. 2). The four RC BChl positions in each monomer were treated separately by fitting the BChl conformations obtained from the crystal structure of *Rba. sphaeroides* RC (PDB id: 1PCR [18]) onto the trajectory-averaged RC BChl conformations described above. This was done in order to minimize the disorder effects of RC BChl placements on the excitonic properties. The excitonic properties display a stronger sensitivity to the conformations of the RC BChls than to the conformations of the antenna BChls. The overall BChl array thus generated was subsequently used for the computation of excitonic properties.

The BChl array that results from MDFF and subsequent averaging exhibits the same bending angle, namely 146°, as seen in the EM density [59]. It had been observed already in an earlier all-atom MD simulation of the *Rba. sphaeroides* RC–LH1–PufX dimer that an initially flat dimer spontaneously bends at the LH1 dimerization

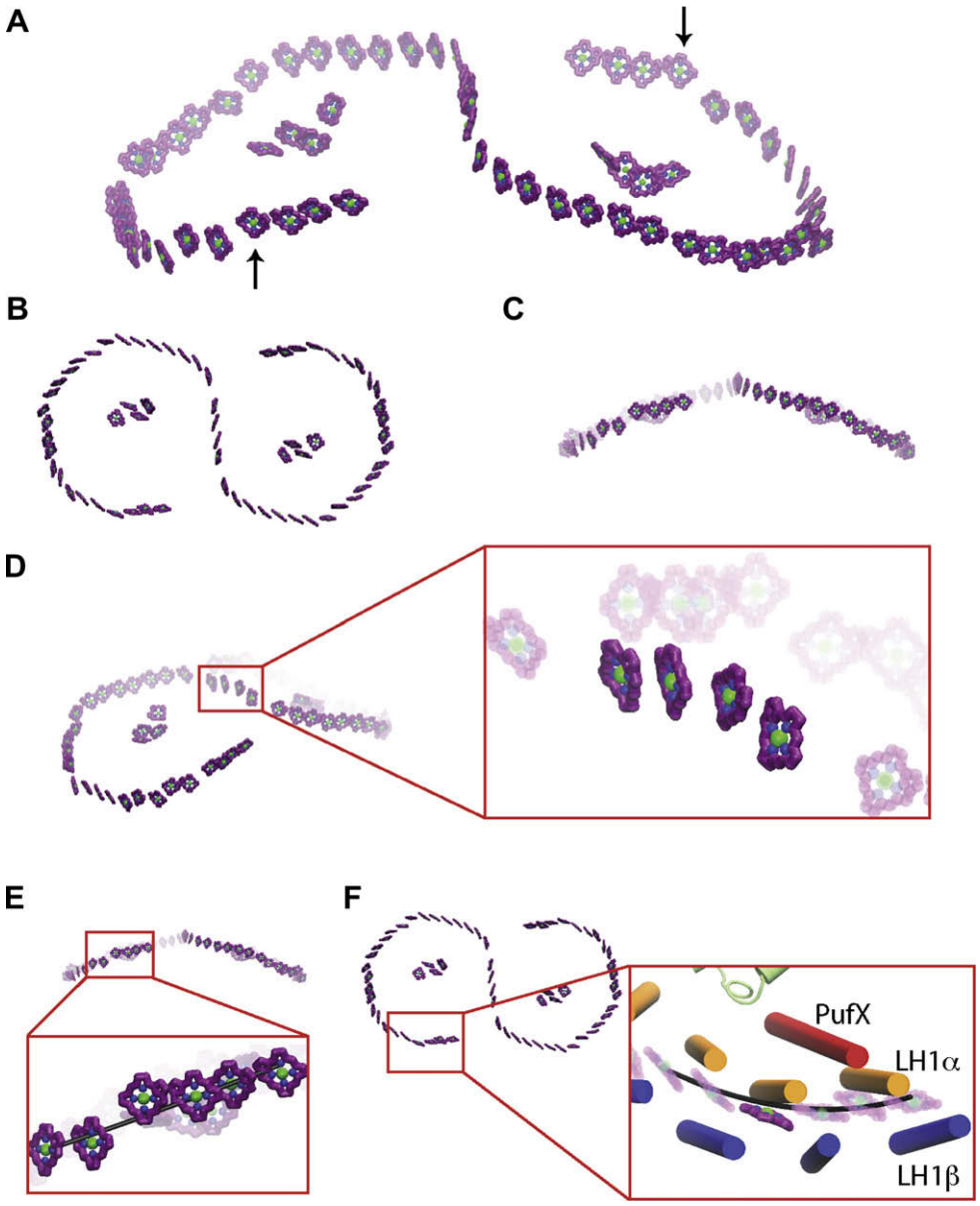

Fig. 2. Detailed views of the BChl array in a dimeric RC–LH1–PufX complex. (A) Shown is the array obtained through MDFF [75] and an EM density map [59] including averaging. The arrows indicate the two BChls in the vicinity of the PufX polypeptides (see also (E) and (F)). Top (B) and side (C) views reveal the relative arrangement of the RC–LH1 monomers in a membrane-bending S-shape. The arrangement of the four BChls at the LH1 dimerization junction is shown in greater detail in (D). As seen in the side view of the membrane plane (E) and the top view (F), the BChl next to the PufX polypeptide (indicated in (A) with arrows) is displaced with respect to the rest of the BChl array (shown as an arc obtained by an elliptical fit). This distortion of the BChl array is likely due to the steric effects of the PufX polypeptide, as suggested in [104–106].

junction [64]. This computationally observed bending is in the same direction as that observed in the cryo-EM map [59]. However, the 146° bending seen in the EM map is more prominent than the one resulting in the MD simulation which measured only 172° [64] (180° corresponds to no bending), the discrepancy being likely due to the short (20 ns) simulation time employed in [64].

A notable feature of the dimeric BChl array resulting from the present MDFF analysis is a distortion in the vicinity of the PufX polypeptide. The BChls closest to the PufX polypeptide (indicated by arrows in Fig. 2A and shown enlarged in Fig. 2E and F) appear to be displaced by approximately 5 Å with respect to the neighboring BChls both in the plane of the BChl array and along its normal. This displacement is consistent with earlier suggestions [104–106] that the interaction between PufX and its nearby BChl distorts the BChl array.

The BChls at the dimerization junction (defined in Fig. 2D) link the LH1 BChls of the two monomers into an S-shaped band. This inter-monomer link as well as the intra-monomer links between BChls lead to a sharing of excitations between the LH1 monomers (and the two RCs) as reported in [50]. Excitation sharing between the two RCs of one dimer as well as between the RCs of neighboring dimers may be responsible for maintaining a high efficiency under high-light conditions. The excitonic properties of the BChl array are discussed in detail in the following section.

3.2. Excitonic structure of the bacteriochlorophyll array

Energy transfer dynamics in the BChl array is closely related to the spectral properties of the excitonic states, both determined by the effective Hamiltonian (Eq. (2)). Specifically, the rate of energy transfer (Eq. (4)) between the RC and the LH1 BChls is dominated by resonant transfer between donor states m and acceptor states n that have the strongest couplings V_{mn}^{DA} (as defined in Eq. (5)) and the best spectral overlaps [45]. Therefore, in order to deter-

mine the energy transfer characteristics of the BChl array the excitonic states must be examined in detail.

In this section, we first present the excitonic spectrum of the BChl array shown in Fig. 3. Then the optical properties (such as oscillator strength) and the delocalization character (such as inverse participation ratio and coherence length, defined below) of the excitonic states presented in Fig. 4 are discussed along with the donor–acceptor excitonic couplings V_{mn}^{DA} relevant for the computation of energy transfer between RC and LH1 BChls as presented in Fig. 5. A comparison is then made between the excitonic properties of monomeric circular and dimeric S-shaped BChl assemblies (cf. Figs. 3 and 5).

The S-shaped dimeric BChl array presented in Fig. 2A displays excitonic properties that are notably different from those of the circularly symmetric RC–LH1 monomeric complexes studied previously [38,39,77,45,78,9]. For a comparison of the excitonic properties of circular and S-shaped BChl arrays, effective Hamiltonians were constructed according to Eq. (2) with identical parameters for inter-BChl couplings and site energies. The range of the resulting excitation energy levels are similar for circular and S-shaped BChl arrays as seen in Fig. 3 (for clarity only the lower half of the exciton band is shown). Notably, the doubly-degenerate energy levels present in the spectrum of the circular RC–LH1 complexes [39,45] lose their degeneracy in the case of the S-shaped complex as a consequence of the lost circular symmetry.

The spread of excitonic states over the dimeric BChl array is shown in Fig. 4, illustrating the significant delocalization of excitons. The number of pigments over which an excitonic state is delocalized at a finite temperature is given by the coherence length [107,49] (see Appendix; Eq. (8)). For room temperature, one obtains a coherence length of 6.5 BChls for the dimeric LH1 BChl aggregate which is similar to the coherence length of LH2 BChls reported in [49]. Thus, thermal effects limit the delocalization of the excitation to only a few BChls rather than to the entire array as seen at zero temperature.

The contribution of each excitonic state m to the absorption spectrum of the BChl array is given by its oscillator strength

$$\alpha_m = |\sum_k c_{m,k}\mathbf{d}_\mathbf{k}|^2 \tag{6}$$

as displayed in Fig. 4. Here $c_{m,k}$ are the eigenvectors of the Hamiltonian (Eq. (2)). A comparison of Figs. 4 and 5 shows that the states m with the strongest couplings V_{m1}^{DA} between LH1 and RC (for the RC, $n > 1$ states contribute minimally to couplings and energy transfer) also exhibit the strongest oscillator strength. For the circular complex the largest oscillator strength is carried by the doubly-degenerate levels $m = 2, 3$, whereas the lowest level $m = 1$, due to symmetry, carries almost no oscillator strength [45]. However, for the S-shaped dimeric complex, symmetry-induced energy degeneracies are broken (cf. Fig. 3) and the lowest level $m = 1$ accrues non-zero oscillator strength, whereas the highest oscillator strength is carried by the non-degenerate $m = 3$ state shown in Fig. 3B; this behavior holds for both the flat dimeric complex considered earlier [50] and the membrane-bending complex shown in Fig. 2. For both circular and S-shaped complexes, the highest oscillator strength stems from the 875 nm (11430 cm^{-1}) state.

The couplings V_{m1}^{DA} between the LH1 excitonic states m and the lowest ($n = 1$) RC excitonic state are shown in Fig. 5. For both the circular and the S-shaped complexes the strongest RC–LH1 couplings measure $|V_{m,1}^{DA}| = 7\ cm^{-1}$ and arise between the lowest ($n = 1$) RC state and LH1 states $m = 2, 3$ for the circular and $m = 3$ for the S-shaped complexes, respectively. Thus, the room temperature excitation energy transfer rate (Eq. (4)) between LH1 and RC is dominated largely by the coupling term V_{m1}^{DA} [45,78,50]. The transfer times computed with the effective Hamiltonian parameters discussed above are 41 ps and 7.4 ps for forward (LH1 → RC) and backward (RC → LH1) transfer, respectively, for the monomeric circular complex, and 51 ps and 8.1 ps for the dimeric S-shaped complex. Both forward and backward excitation transfer rates are similar between the monomeric circular and dimeric S-shaped complexes, since the couplings between the most dominant exciton states are nearly identical between the circular and S-shaped pigment arrays as seen in Fig. 5. The stated transfer times compare favorably with the 'trapping' lifetime of 30–50 ps reported for RC–LH1 complexes [108–111,12] as well as the 'detrapping' probability of about 20% [112–114]. The detrapping probability $p_{\text{detrap}} = \tau_{CS}/(\tau_{CS} + \tau_{(RC\rightarrow LH1)}) = 0.27$ is defined as the probability for an excitation that reaches the RC to 'detrap', i.e., transfer back from the RC to LH1, which happens with a time constant $\tau_{(RC\rightarrow LH1)} = 8.1$ ps as opposed to causing a charge separation at the RC which happens with a time constant $\tau_{CS} = 3$ ps.

From the comparison between circular and S-shaped RC–LH1 complexes presented above we conclude that the presence of PufX, which is responsible for the gap in the BChl ring of each monomer as well as for the dimerization of the RC–LH1 units, has little effect on the spectral properties of RC–LH1 complexes at room tempera-

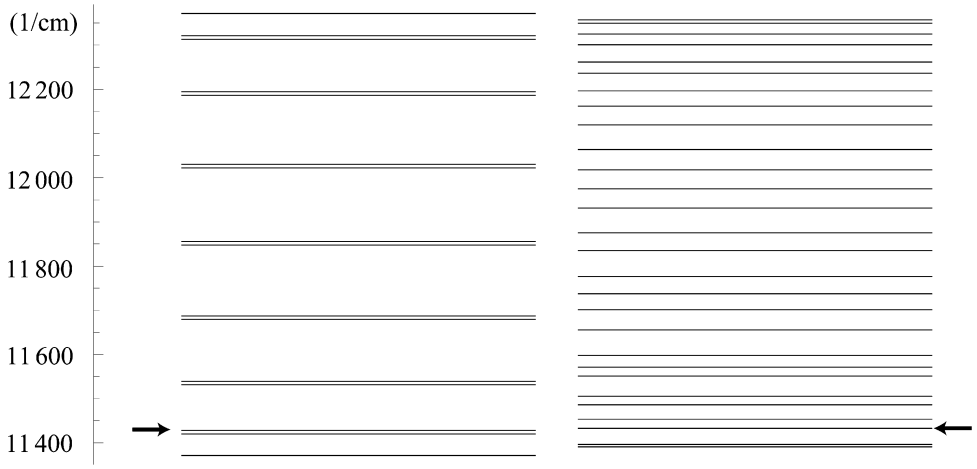

Fig. 3. Exciton bands for monomeric/circular (left) and dimeric/S-shaped (right) LH1 BChl arrays (only the lower half of the bands are shown for clarity). Identical coupling terms and site energies were used for BChls in both effective Hamiltonians. The breaking of circular symmetry lifts the degeneracies (indicated by double lines) of the monomer eigenstates. The highest oscillator strength is carried by the 875 nm states in both cases, which are the doubly degenerate $n = 2, 3$ states for the circular monomer and the non-degenerate $n = 3$ state for the S-shaped dimer (indicated by arrows; see also Fig. 4).

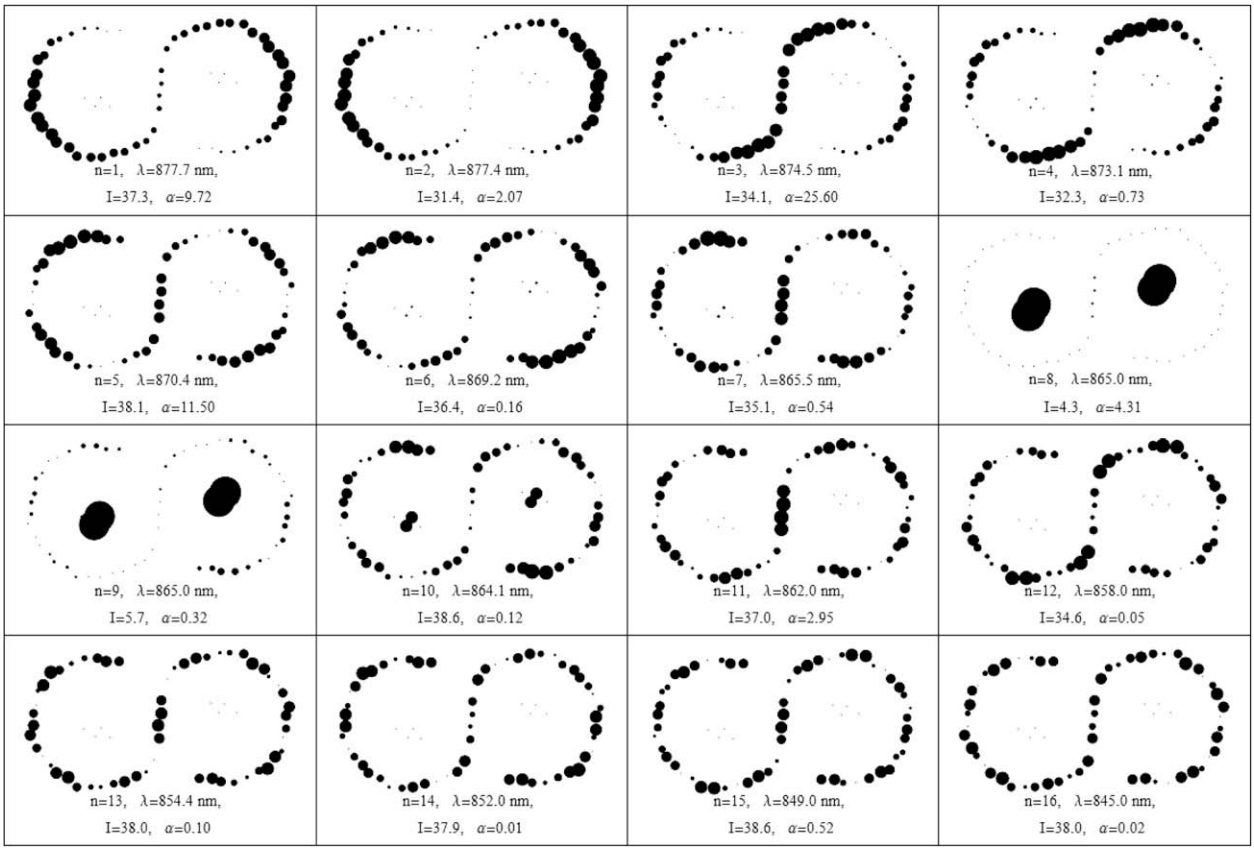

Fig. 4. Spread of the lowest exciton states over the BChl array of the dimeric RC–LH1–PufX complex (cf. Fig. 2). Shown are the occupation probabilities $|c_{n,k}|^2$ for each BChl k for eigenstates $n = 1, \ldots, 16$ (higher states not shown). The area of each circle at a BChl site k is proportional to the occupation probability $|c_{n,k}|^2$ for the state n. Also indicated for each state is the corresponding absorption wavelength λ, the inverse participation ratio I, which is a measure of excitonic delocalization (see Appendix), and the oscillator strength α. The maximum oscillator strength is carried by state $n = 3$ which absorbs at 875 nm.

ture. The resonant energy transfer between peripheral antennae and RCs is mostly unaffected by the dimerization and the out-of-plane distortion of the BChl array. This is reminiscent of the observation that distortions of pigment geometry away from the RC has little effect on excitation transfer characteristics at room temperature [115]. Accordingly, evolutionary adaptation to the presence of the PufX polypeptide, which likely facilitates efficient quinone transport, was easily realized without counter-balancing spectral tuning of light-harvesting proteins, a tuning that would have required structural changes to the constituent α/β-apoproteins.

4. Discussion

The membrane curvature induced spontaneously by the constituent pigment–protein complexes of the PSU seems to have two related functions. Firstly, curved photosynthetic membranes can accommodate a greater number of pigments within a given volume. In fact, the thylakoid membrane of the evolutionarily more complex plants and cyanobacteria shows a much more elaborate organization of curvature with an even more efficient use of available volume. Secondly, the induced curvature of the constituent complexes can facilitate the assembly of the photosynthetic vesicles by enforcing co-location of equally curved building blocks as a recent Monte Carlo study has shown [73] and as had been argued in [64]; co-location is entropically unfavorable but complementary curvature can be favored energetically such that the overall free energy balance for co-location becomes favorable.

The membrane-bending curvature induced by proteins effectively attracts them toward one another in the membrane, causing in the present case pigment–protein complexes to assemble into clusters as opposed to being scattered in the membrane. The cluster formation is crucial for maintaining high efficiency of the light-harvesting process [11]. Gaps greater than 3–4 nm between pigment–protein complexes, e.g., LH2s, would lead to a significant drop of efficiency in the transfer of excitation due to internal conversion or fluorescence that occur on a nanosecond timescale.

The rationale for the bending of S-shaped dimers in *Rba. sphaeroides* is not fully understood. A bending angle of 146° is consistent with the 70 nm average vesicle size and contributes to the aforementioned vesicle formation process through induced curvature. The dimeric RC–LH1–PufX complexes further organize into linear arrays [53]. This linear arrangement of dimers may be guided by direct surface interactions between neighboring LH1 units or through indirect interactions due to the lipid environment [50,64]. Two possible reasons for the formation of the linear dimer arrays of RC–LH1–PufX complexes have been proposed in [50]. First, significant excitation sharing between RCs was observed computationally which may increase light-harvesting efficiency under high-light conditions. Second, the linear dimer arrays surrounded by a layer of lipids may provide 'highways' for fast quinone transport to the bc_1 complexes located at the edge of the vesicle [50]. This role could be supported by the opening in the LH1 BChl 'ring' caused by the presence of PufX. The PufX polypeptide is reported to be essential for photosynthetic growth as well as for the formation of dimeric core complexes [55,59].

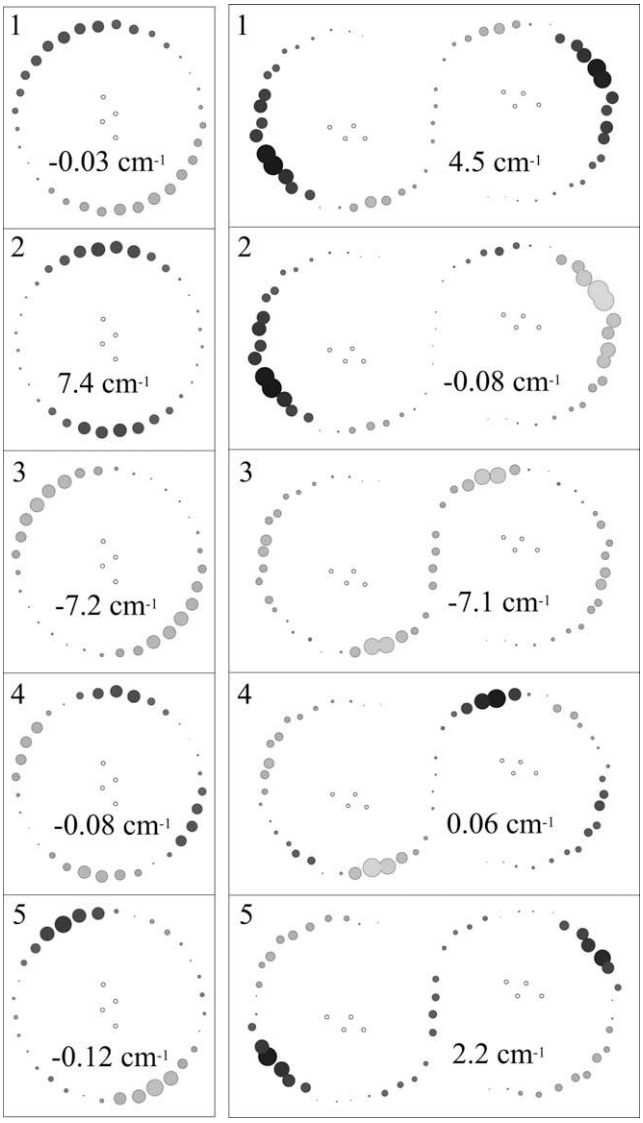

Fig. 5. Excitonic couplings V_{n1}^{DA} (Eq. (5)) between the excitonic states n of the LH1 BChl array and the lowest RC excitonic state for monomeric (left) and dimeric (right) complexes. The contribution of each LH1 BChl is indicated by the area of the respective circle. Positive contributions are shown in dark gray, negative ones in light gray. The states with high oscillator strength (cf. Fig. 4) are most strongly coupled to the lowest RC state.

Neither the bending of the BChl array nor the structural discontinuity that results from the gap caused by PufX has a significant effect on the excitonic properties of the RC–LH1 complex as compared to excitonic properties of monomeric circular units as found in other purple bacteria. This suggests that effective excitation transfer can be accommodated amid other essential processes such as vesicle assembly and quinone diffusion. Therefore, the role of PufX and dimer bending is very likely structural, and not for optimizing the excitation transfer aspect of chromatophore function. It might, in fact, be true that optimization of assembly comes at the price of lowered harvesting efficiency as the monomeric circular LH1–RC complex has a slightly faster transfer rate (1/41 ps) than the dimeric S-shaped complex (1/51 ps). In comparison, photosystem I of oxygenic photosynthesis is also robust against deformations of pigment geometry while also displaying limited optimization of architecture [115–117]. However, the modular architecture of the purple bacterial photosynthetic unit requires that comparisons of efficiency should be made not on the scale of individual proteins but instead on the scale of an entire chromatophore vesicle taking into account cooperation between multiple proteins. Such a comparison is beyond the scope of the current study. Light-harvesting optimality at a system level is not yet well understood in purple bacteria.

Beyond a high packing density of the constituent pigment-clusters and the spectral tuning of the excitonic levels needed for resonant energy transfer, the excitation transfer process shows robustness and insensitivity to geometric detail. This conclusion is in agreement with very early work of Oppenheimer [2], Arnold and Oppenheimer [3] and Duysens [6].

Acknowledgements

The authors would like to thank D. Chandler, J. Gumbart, C.B. Harrison, P.A. Bullough, and R. van Grondelle for useful discussions. This work was supported by National Science Foundation grant MCB0744057 and National Institutes of Health grant P41-RR05969 (to K.S.) as well as the Biotechnology and Biological Research Council, UK (grant to C.N.H.). Computer time was provided at the National Center for Supercomputing Applications and the Texas Advanced Computing Center via a NSF Large Resources Allocation Committee grant MCA93S028. Molecular images in this paper were generated with VMD [118].

Appendix

In this appendix, we define the inverse participation ratio and the coherence length as measures of delocalization of excitonic states [107,49].

The lowest 16 eigenstates of the effective Hamiltonian given by Eq. (2) for the entire dimeric complex (consisting of a total of 64 BChls: 56 LH1 BChls and four BChls for each of the two RCs) are shown in Fig. 4. For each eigenstate n the occupation probabilities $|c_{n,k}|^2$ for each BChl k are shown together with the absorption wavelength λ corresponding to that state. The occupation probabilities directly determine the inverse participation ratio [107,49]

$$I_n = 1 \Big/ \sum_k |c_{n,k}|^4 \tag{7}$$

of the state n which is a measure of excitonic delocalization for that state, corresponding approximately to the number of BChls over which an excitonic state is distributed. The inverse participation ratio is larger for eigenstates that display larger delocalization over pigments. The low lying excitonic states all have significant delocalization with the exception of the two degenerate states at 865 nm ($n = 8, 9$) corresponding to the special pair absorption at each monomer.

Thermal disorder effects reduce the number of pigments an excitation is distributed over. Taking into account the effects of disorder, a measure of excitonic delocalization is provided by the coherence length

$$L_\rho = \left(\sum_{ij} |\rho_{ij}|\right)^2 \Big/ \left(N \sum_{ij} |\rho_{ij}|^2\right), \tag{8}$$

where

$$\rho_{ij} = \sum_n c_{n,i}^* c_{n,j} \exp(-(E_n - E_1)/(k_B T)) \tag{9}$$

is the reduced exciton density matrix [107,49].

References

[1] R. Emerson, A. Arnold, J. Gen. Physiol. 16 (1932) 191.

[2] J.R. Oppenheimer, in: Proceedings of the American Physical Society, Phys. Rev., vol. 60, 1941, p. 158.
[3] W. Arnold, J.R. Oppenheimer, J. Gen. Physiol. 33 (1950) 423.
[4] T. Förster, Ann. Phys. (Leipzig) 2 (1948) 55.
[5] D. Dexter, J. Chem. Phys. 21 (1953) 836.
[6] L.N.M. Duysens, Ph.D. Thesis, University of Utrecht, 1952.
[7] Govindjee, in: M. Yunus, U. Pathre, P. Mohanty (Eds.), Probing Photosynthesis Mechanisms Regulation and Adaptation, Taylor and Francis, New York, 2000, p. 9.
[8] R.E. Blankenship, Molecular Mechanisms of Photosynthesis, Blackwell Science, Malden, MA, 2002.
[9] X. Hu, T. Ritz, A. Damjanović, F. Autenrieth, K. Schulten, Quart. Rev. Biophys. 35 (2002) 1.
[10] T. Ritz, A. Damjanović, K. Schulten, ChemPhysChem 3 (2002) 243.
[11] M. Şener, K. Schulten, in: D.L. Andrews (Ed.), Energy Harvesting Materials, World Scientific, Singapore, 2005, p. 1.
[12] R.J. Cogdell, A. Gall, J. Köhler, Quart. Rev. Biophys. 39 (2006) 227.
[13] I. Kosztin, K. Schulten, in: T. Aartsma, J. Matysik (Eds.), Biophysical Techniques in Photosynthesis II, Advances in Photosynthesis and Respiration, vol. 26, Springer, Dordrecht, 2008, p. 445.
[14] M.K. Şener, K. Schulten, in: C.N. Hunter, F. Daldal, M.C. Thurnauer, J.T. Beatty (Eds.), The Purple Phototrophic Bacteria, Advances in Photosynthesis and Respiration, vol. 28, Springer, 2008, p. 275.
[15] J. Xiong, W.M. Fischer, K. Inoue, M. Nakahara, C.E. Bauer, Science 289 (2000) 1724.
[16] J. Deisenhofer, O. Epp, K. Mikki, R. Huber, H. Michel, Nature 318 (1985) 618.
[17] J. Allen, T. Yeates, H. Komiya, D. Rees, Proc. Natl. Acad. Sci. USA 84 (1987) 6162.
[18] U. Ermler, G. Fritzsch, S.K. Buchanan, H. Michel, Structure 2 (1994) 925.
[19] A. Camara-Artigas, D. Brune, J.P. Allen, Proc. Natl. Acad. Sci. USA 99 (2002) 11055.
[20] D. Fotiadis, P. Qian, A. Philippsen, P.A. Bullough, A. Engel, C.N. Hunter, J. Biol. Chem. 279 (2004) 2063.
[21] G. McDermott, S.M. Prince, A.A. Freer, A.M. Hawthornthwaite-Lawless, M.Z. Papiz, R.J. Cogdell, N.W. Isaacs, Nature 374 (1995) 517.
[22] S. Karrasch, P. Bullough, R. Ghosh, EMBO J. 14 (1995) 631.
[23] X. Hu, D. Xu, K. Hamer, K. Schulten, J. Koepke, H. Michel, Prot. Sci. 4 (1995) 1670.
[24] J. Koepke, X. Hu, C. Muenke, K. Schulten, H. Michel, Structure 4 (1996) 581.
[25] M.J. Conroy, W. Westerhuis, P.S. Parkes-Loach, P.A. Loach, C.N. Hunter, M.P. Williamson, J. Mol. Biol. 298 (2000) 83.
[26] A.W. Roszak, T. Howard, J. Southall, A.T. Gardiner, C.J. Law, N.W. Isaacs, R.J. Cogdell, Science 302 (2003) 1969.
[27] M.Z. Papiz, S.M. Prince, T. Howard, R.J. Cogdell, N.W. Isaacs, J. Mol. Biol. 326 (2003) 1523.
[28] H. Treutlein, K. Schulten, J. Deisenhofer, H. Michel, A. Brünger, M. Karplus, in: J. Breton, A. Verméglio (Eds.), The Photosynthetic Bacterial Reaction Center: Structure and Dynamics, NATO Sci. Ser. A, vol. 149, Plenum, New York, 1988, p. 139.
[29] H. Treutlein, K. Schulten, C. Niedermeier, J. Deisenhofer, H. Michel, D. Devault, in: J. Breton, A. Verméglio (Eds.), The Photosynthetic Bacterial Reaction Center: Structure and Dynamics, NATO Sci. Ser. A, vol. 149, Plenum, New York, 1988, p. 369.
[30] K. Schulten, M. Tesch, Chem. Phys. 158 (1991) 421.
[31] M. Nonella, K. Schultenm, J. Phys. Chem. 95 (1991) 2059.
[32] R.W. Visschers, M.C. Chang, F. van Mourik, P.S. Parkes-Loach, B.A. Heller, P.A. Loach, R. van Grondelle, Biochemistry 30 (1991) 5734.
[33] D. Xu, K. Schulten, Chem. Phys. 182 (1994) 91.
[34] R. van Grondelle, J.P. Dekker, T. Gillbro, V. Sundström, Biochim. Biophys. Acta 1187 (1994) 1.
[35] L.M.P. Beekman, F. van Mourik, M.R. Jones, H.M. Visser, C.N. Hunter, R. van Grondelle, Biochemistry 33 (1994) 3143.
[36] S. Mukamel, Principles of Nonlinear Optical Spectroscopy, Oxford University Press, New York, 1995.
[37] X. Hu, T. Ritz, A. Damjanović, K. Schulten, J. Phys. Chem. B 101 (1997) 3854.
[38] T. Ritz, X. Hu, A. Damjanović, K. Schulten, J. Lumin. 76–77 (1998) 310.
[39] X. Hu, A. Damjanović, T. Ritz, K. Schulten, Proc. Natl. Acad. Sci. USA 95 (1998) 5935.
[40] X. Hu, K. Schulten, Biophys. J. 75 (1998) 683.
[41] B.P. Krueger, G.D. Scholes, G.R. Fleming, J. Phys. Chem. B 102 (1998) 5378.
[42] V. Sundström, T. Pullerits, R. van Grondelle, J. Phys. Chem. B 103 (1999) 2327.
[43] G. Scholes, I. Gould, R. Cogdell, G. Fleming, J. Phys. Chem. B 103 (1999) 2543.
[44] S. Tretiak, C. Middleton, V. Chernyak, S. Mukamel, J. Phys. Chem. B 104 (2000) 9540.
[45] A. Damjanović, T. Ritz, K. Schulten, Int. J. Quantum Chem. 77 (2000) 139.
[46] A. Damjanović, T. Ritz, K. Schulten, Biophys. J. 79 (2000) 1695.
[47] T. Ritz, A. Damjanović, K. Schulten, J. Zhang, Y. Koyama, Photosynth. Res. 66 (2000) 125.
[48] M. Sener, K. Schulten, Phys. Rev. E 65 (2002) 031916 (12pp.).
[49] A. Damjanović, I. Kosztin, U. Kleinekathoefer, K. Schulten, Phys. Rev. E 65 (2002) 031919 (24pp.).
[50] M.K. Sener, J.D. Olsen, C.N. Hunter, K. Schulten, Proc. Natl. Acad. Sci. USA 104 (2007) 15723.
[51] C. Jungas, J. Ranck, J. Rigaud, P. Joliot, A. Verméglio, EMBO J. 18 (1999) 534.
[52] S.J. Jamieson, P. Wang, P. Qian, J.Y. Kirkland, M.J. Conroy, C.N. Hunter, P.A. Bullough, J. Mol. Biol. 21 (2002) 3927.
[53] S. Bahatyrova, R.N. Frese, C.A. Siebert, J.D. Olsen, K.O. van der Werf, R. van Grondelle, R.A. Niederman, P.A. Bullough, C. Otto, C.N. Hunter, Nature 430 (2004) 1058.
[54] S. Scheuring, J.N. Sturgis, V. Prima, A. Bernadac, D. Levy, J.-L. Rigaud, Proc. Natl. Acad. Sci. USA 91 (2004) 11293.
[55] C.A. Siebert, P. Qian, D. Fotiadis, A. Engel, C.N. Hunter, P.A. Bullough, EMBO J. 23 (2004) 690.
[56] R.N. Frese, C.A. Siebert, R.A. Niederman, C.N. Hunter, C. Otto, R. van Grondelle, Proc. Natl. Acad. Sci. USA 101 (2004) 17994.
[57] P. Qian, C.N. Hunter, P.A. Bullough, J. Mol. Biol. 349 (2005) 948.
[58] S. Scheuring, D. Lévy, J.-L. Rigaud, Biochim. Biophys. Acta 1712 (2005) 109.
[59] P. Qian, P.A. Bullough, C.N. Hunter, J. Biol. Chem. 283 (2008) 14002.
[60] T. Geyer, V. Helms, Biophys. J. 91 (2006) 921.
[61] T. Geyer, V. Helms, Biophys. J. 91 (2006) 927.
[62] T. Geyer, F. Lauck, V. Helms, J. Biotechnol. 129 (2) (2007) 212.
[63] T. Geyer, Biophys. J. 93 (2007) 4374.
[64] D. Chandler, J. Hsin, C.B. Harrison, J. Gumbart, K. Schulten, Biophys. J. 95 (2008) 2822.
[65] A.R. Crofts, C.A. Wraight, Biochim. Biophys. Acta 726 (1983) 149.
[66] F. Velasco, A.R. Crofts, Biochem. Soc. Trans. 19 (1991) 588.
[67] R.B. Gennis, B. Barquera, B. Hacker, S.R.V. Doren, S. Arnaud, A.R. Crofts, E. Davidson, K.A. Gray, F. Daldal, J. Bioenerg. Biomembr. 25 (1993) 195.
[68] D. Xia, C.-A. Yu, H. Kim, J.-Z. Xia, A.M. Kachurin, L. Zhang, L. Yu, J. Deisenhofer, Science 277 (1997) 60.
[69] W. Junge, H. Lill, S. Engelbrecht, Trends Biochem. Sci. 22 (1997) 420.
[70] R.H. Fillingame, W. Jiang, O.Y. Dmitriev, J. Exp. Biol. 203 (2000) 9.
[71] R.H. Fillingame, Nat. Struct. Biol. 7 (2000) 1002.
[72] M. Strauss, G. Hofhaus, R.R. Schröder, W. Kühlbrandt, EMBO J. 27 (2008) 1154.
[73] R.N. Frese, J.C. Pàmies, J.D. Olsen, S. Bahatyrova, C.D. van der Weij-de Wit, T.J. Aartsma, C. Otto, C.N. Hunter, D. Frenkel, R. van Grondelle, Biophys. J. 94 (2008) 640.
[74] J. Hsin, J. Gumbart, L.G. Trabuco, E. Villa, P. Qian, C.N. Hunter, P.A. Bullough, K. Schulten, Biophys. J., submitted for publication.
[75] L.G. Trabuco, E. Villa, K. Mitra, J. Frank, K. Schulten, Structure 16 (2008) 673.
[76] E. Villa, J. Sengupta, L.G. Trabuco, J. LeBarron, W.T. Baxter, T.R. Shaikh, R.A. Grassucci, P. Nissen, M. Ehrenberg, K. Schulten, J. Frank, Proc. Natl. Acad. Sci. USA 106 (2009) 1063.
[77] A. Damjanović, T. Ritz, K. Schulten, Phys. Rev. E 59 (1999) 3293.
[78] T. Ritz, S. Park, K. Schulten, J. Phys. Chem. B 105 (2001) 8259.
[79] M. Yang, G.R. Fleming, Chem. Phys. 282 (2002) 163.
[80] D. Rutkauskas, V.I. Novoderezhkin, R.J. Cogdell, R. van Grondelle, Biophys. J. 88 (2005) 422.
[81] R. van Grondelle, V.I. Novoderezhkin, Phys. Chem. Chem. Phys. 8 (2006) 793.
[82] Z.Y. Wang, K. Gokan, M. Kobayashi, T. Nozawa, J. Mol. Biol. 347 (2005) 465.
[83] R.B. Tunnicliffe, E.C. Ratcliffe, C.N. Hunter, M.P. Williamson, FEBS Lett. 580 (2006) 6967.
[84] W. Wriggers, R.A. Milligan, J.A. McCammon, J. Struct. Biol. 125 (1999) 185.
[85] J.C. Phillips, R. Braun, W. Wang, J. Gumbart, E. Tajkhorshid, E. Villa, C. Chipot, R.D. Skeel, L. Kale, K. Schulten, J. Comput. Chem. 26 (2005) 1781.
[86] B. Isralewitz, M. Gao, K. Schulten, Curr. Opin. Struct. Biol. 11 (2001) 224.
[87] M. Sotomayor, K. Schulten, Science 316 (2007) 1144.
[88] D. Wells, V. Abramkina, A. Aksimentiev, J. Chem. Phys. 127 (2007) 125101.
[89] A. MacKerell Jr., D. Bashford, M. Bellott, R.L. Dunbrack Jr., J. Evanseck, M.J. Field, S. Fischer, J. Gao, H. Guo, S. Ha, D. Joseph, L. Kuchnir, K. Kuczera, F.T.K. Lau, C. Mattos, S. Michnick, T. Ngo, D.T. Nguyen, B. Prodhom, I.W.E. Reiher, B. Roux, M. Schlenkrich, J. Smith, R. Stote, J. Straub, M. Watanabe, J. Wiorkiewicz-Kuczera, D. Yin, M. Karplus, J. Phys. Chem. B 102 (1998) 3586.
[90] A.D. MacKerell Jr., M. Feig, C.L. Brooks III, J. Comput. Chem. 25 (2004) 1400.
[91] W.L. Jorgensen, J. Chandrasekhar, J.D. Madura, R.W. Impey, M.L. Klein, J. Chem. Phys. 79 (1983) 926.
[92] T. Schlick, R. Skeel, A. Brünger, L. Kalé, J.A. Board Jr., J. Hermans, K. Schulten, J. Comput. Phys 151 (1999) 9.
[93] H. Scheer, Chlorophylls, CRC Press, Boca Raton, Florida, 1991.
[94] J. Eccles, B. Honig, K. Schulten, Biophys. J. 53 (1988) 137.
[95] M.H.C. Koolhaas, R.N. Frese, G.J.S. Fowler, T.S. Bibby, S. Georgakopoulou, G. van der Zwan, C.N. Hunter, R. van Grondelle, Biochemistry 37 (1998) 4693.
[96] M. Groot, J. Yu, R. Agarwal, J.R. Norris, G.R. Fleming, J. Phys. Chem. B 102 (1998) 5923.
[97] R.S. Knox, B.Q. Spring, Photochem. Photobiol. 77 (2003) 497.
[98] M.G. Cory, M.C. Zerner, X. Hu, K. Schulten, J. Phys. Chem. B 102 (1998) 7640.
[99] H. Sumi, J. Phys. Chem. B 103 (1999) 252.
[100] S. Jang, M.D. Newton, R.J. Silbey, Phys. Rev. Lett. 92 (2004) 218301 (4pp.).
[101] G.D. Scholes, Ann. Rev. Phys. Chem. 54 (2003) 57.
[102] W.M. Zhang, T. Meier, V. Chernyak, S. Mukamel, J. Chem. Phys. 108 (1998) 7763.
[103] V. Novoderezhkin, R. van Grondelle, J. Phys. Chem. B 106 (2002) 6025.
[104] C.J. Law, J. Chen, P.S. Parkes-Loach, P.A. Loach, Photosynth. Res. 75 (2003) 193.
[105] M. Aklujkar, J.T. Beatty, Arch. Biochem. Biophys. 443 (2005) 21.
[106] M. Aklujkar, J.T. Beatty, Photosynth. Res. 88 (2006) 159.
[107] T. Meier, Y. Zhao, V. Chernyak, S. Mukamel, J. Chem. Phys. 107 (1997) 3876.
[108] V. Sundström, R. van Grondelle, H. Bergström, E. Aakesson, T. Gillbro, Biochim. Biophys. Acta – Bioener. 851 (1986) 431.
[109] H. Bergström, R. van Grondelle, V. Sundström, FEBS Lett. 250 (1989) 503.
[110] K.J. Visscher, H. Bergstrom, V. Sundström, C. Hunter, R. van Grondelle, Photosynth. Res. 22 (1989) 211.

[111] A. Freiberg, J.P. Allen, J.C. Williams, N.W. Woodbury, Photosynth. Res. 48 (1996) 309.
[112] K. Timpmann, A. Freiberg, V. Sundström, Chem. Phys. 194 (1995) 275.
[113] K. Bernhardt, H.-W. Trissl, Biochim. Biophys. Acta 1457 (2000) 1.
[114] J. Amesz, S. Neerken, Photosynth. Res. 73 (2002) 73.
[115] M.K. Şener, D. Lu, T. Ritz, S. Park, P. Fromme, K. Schulten, J. Phys. Chem. B 106 (2002) 7948.
[116] M.K. Şener, S. Park, D. Lu, A. Damjanović, T. Ritz, P. Fromme, K. Schulten, J. Chem. Phys. 120 (2004) 11183.
[117] D. Bruce, S. Vasil'ev, Plant Cell 16 (2004) 3059.
[118] W. Humphrey, A. Dalke, K. Schulten, J. Mol. Graph. 14 (1996) 33.